Peer-reviewed version available at *Energies* **2020**, *13*, 919; doi:10.3390/en13040919

Article

Effects of Combination Impeller on the Flow Field and External Performance of an Aero-fuel Centrifugal Pump

Jia Li [1,*], Xin Wang [2], Yue Wang [3], Wancheng Wang [4], Baibing Chen [5] , and Xiaolong Chen [6]

[1] School of Construction Machinery, Chang'an University; lijia@chd.edu.cn
[2] School of Construction Machinery, Chang'an University; wangxin@chd.edu.cn
[3] AECC Xi'an Power Control Technology Co. LTD; wangyue1018@126.com
[4] AECC Xi'an Power Control Technology Co. LTD; company113@163.cn
[5] Xian Modern Control Technology Research Institute; gerrard75166@126.com
[6] Xian Modern Control Technology Research Institute; jjyyvivi@126.com
* Correspondence: lijia@chd.edu.cn; Tel.: (Xi'an, 710064, China) +86-18066591366 (F.L.)

Abstract: Aero-fuel centrifugal pumps are important power plants in aero-engines. Unlike most of the existing centrifugal pumps, a combination impeller is integrated with the pump to improve its performance. First, the critical geometrical parameters of combination impeller and volute are given. Then, the effects of combination impeller on flow characteristics inside the impeller and volute are clarified by comparing simulation results with that of the conventional impeller, where the effectiveness of selected numerical method is validated by an acceptable agreement between simulation and experiment. Finally, the experiment is performed to test the external performance of studied pump. A significant feature of this study is that the flow characteristics are significantly ameliorated by reducing the flow losses emerged in impeller inlet, impeller outlet and volute tongue. Correspondingly, the head and efficiency of combination impeller are higher with comparison to conventional impeller. Consequently, it is a promising approach in ameliorating flow field and improving external performance by applying a combination impeller to an aero-fuel centrifugal pump.

Keywords: aero-fuel centrifugal pump; combination impeller; flow loss; flow characteristics; head and efficiency

1. Introduction

The introduction should briefly place the study in a broad context and highlight why it is important. It should define the purpose of the work and its significance. The current state of the research field should be reviewed carefully and key publications cited. Please highlight controversial and diverging hypotheses when necessary. Finally, briefly mention the main aim of the work and highlight the principal conclusions. As far as possible, please keep the introduction comprehensible to scientists outside your particular field of research. References should be numbered in order of appearance and indicated by a numeral or numerals in square brackets, e.g., [1] or [2, 3], or [4–6]. See the end of the document for further details on references.

As an energy consuming turbo-machine, the centrifugal pump is of urgent demand for energy source in the industry due to its energy-saving potential. It has been widely used for many applications, such as aviation and aerospace [1, 2], micro-hydro-power plants [3, 4], wind power generation [5, 6], petroleum process [7] and agriculture irrigation [8]. Importantly, there is a growing recognition in the field of improving performance of an aero-fuel centrifugal pump associated with a military aero-engine [9]. The centrifugal pump is usually used as the pre-pressurization pump for the fuel system of an aero-engine. The impeller structure is critical to utilize the energy for improving the pump performance, where the fuel is pumped to take the energy from inlet to the

volute in form of kinetic energy and static pressure. Therefore, the critical issues for performance of an aero-fuel centrifugal pump with the proposed combination impeller need to be specially considered, which are normally beyond what a conventional method can provide.

As for the vital role of an impeller for a centrifugal pump, many investigations on impeller design and performance prediction have been carried out. In [10], a review on two phase performances from various centrifugal pumps designs is presented, mainly based on experimental results. It is still useful to perform experimental two phase flow studies. In [11], a centrifugal pump performance prediction method based on the BP neural network is proposed. It indicates that the proposed method can realize hydraulic performance prediction during the design process of a centrifugal pump. In [12], an additional splitter blade is presented and integrated in a centrifugal pump. It shows that a higher performance is obtained than that of the pump with a conventional impeller. Moreover, the effect of the geometrical parameters of impeller on performance has been conducted. In [13], the efficiency can be changed significantly with a slightly change of impeller axial clearance. In [14], the head and cavitation performance of the centrifugal pump are affected by the blade angle. In addition, an optimum value of hydraulic efficiency can be obtained when adjusting the impeller shroud radius [15]. Therefore, it is essential and important to characterize the performance of an aero-fuel centrifugal pump with different impellers under various operation conditions. As one of the motivations in this paper, the effect of the proposed combination impeller on external performance is investigated to ensure its superiority.

Furthermore, in order to realize the effects of an impeller on the fluid characteristics inside the centrifugal pump, numerical simulation has been investigated. The effect of impeller's blade numbers on the pump efficiency is studied in [16] by using a commercial CFD code. Three different turbulence models are selected to simulate the flow fields with different blade numbers. In [17], by changing impeller outlet angle and impeller passage width, the 3-D flow characteristics are achieved numerically for a centrifugal pump to analyze its pump performance, and acceptable agreement has been showed from the numerical and experimental results. For the complex flow characteristics occurring in the impeller, it usually has an adverse effect on cavitation performance [18, 19]. In [18], the cavitation can be induced due to the serious hydraulic shock acting on the blade under some extreme conditions. The impeller geometrical parameters are important factors to improve anti-cavitation performance for centrifugal pump. As indicated in [19], the effect of inlet blade angle is obviously and sensitive on anti-cavitation performance. In general, there may cause a certain secondary loss, friction loss, or mixing loss inside impeller. So, a particular impeller can improve the reliability of pump operation by reducing the flow losses. From this review, it is very important for a centrifugal pump to understand its flow characteristics. This presents another motivation for this paper which aims to realize the effects of a combination impeller on detailed flow characteristics by an effective numerical simulation method, while comparing with experimental data.

Although extensive studies have been conducted for the effect of an impeller on the flow field and external performance, there are some difficulties that need to be addressed. 1) The flow field and external performance are mainly regulated by the impeller, and the geometrical parameters are treated as the vital factors. So, it still need investigate on the effect of an impeller [20-23]. 2) In order to improve hydraulic efficiency and maintain system stability, it is a common and conventional method to solve serious flow problems by equipping an inducer before an impeller [24, 25]. Only few of them, apply a combination impeller on a centrifugal pump. 3) The combination impeller has not been specifically used for an aero-fuel centrifugal pump, and it has not considered the viscosity of aero-fuel [26], the operation conditions under high-pressure and large flow rate [27].

In an attempt to overcome the above-mentioned difficulties, this paper presents an aero-fuel centrifugal pump with a combination impeller applied to an aero-engine. The aim is to obtain the detailed flow characteristics and optimal external performances by numerical simulation and experiment. It will be beneficial to have an aero-fuel centrifugal pump with the capability of suppressing serious flow instabilities under extreme conditions by equipping a combination impeller.

2. Research model description

2.1. Objective

The aero-fuel centrifugal pump studied in this paper is a single-stage single-suction centrifugal pump with operating at a large flow rate. It is used as the pre-pressurization pump in the fuel system of an aero-engine for transporting fuel (RP-3) [1, 9]. Aero-fuel (RP-3) is selected as the initial intended working fluid for the simulation and experiment to keep the results precise and approved. The main technical requirements of the studied pump at the nominal operating point are listed in Table 1.

Table 1. The technical requirements at the nominal operating point

Performance parameters	Value
Q_d(L/h)	77,000
H(m)	137
n_s	106.6
η_v	0.65
N_d(r/min)	8,000

The operating range of the pump is determined by the flight-envelope of aero-engine, including: rotor speed, flow rate, inlet and outlet pressure. A shaft speed N_d of 8000RPM and flow rate Q_d of 77000L/h are set as the nominal operating point. The pump needs to be capable of pumping fuel at the outlet pressure P_c of 0.956MPa. The density of the aero-fuel (RP-3) is 779kg/m^3 when operating at 20°C.

2.2. Configuration and layout of the research model

The final pump configuration is shown in Fig. 1. The pump essentially consists of a combination impeller, a volute, a diffuser and a pump drive shaft. The combination impeller is placed in middle of the pump. The fuel is transported and accelerated by the impeller in the counterclockwise circumferential direction. Then, around the outlet line of impeller, the fuel is pumped out to the volute by dint of centrifugal force. Finally, the fuel is decelerated in the following diffuser before entering the main-fuel pump of fuel system.

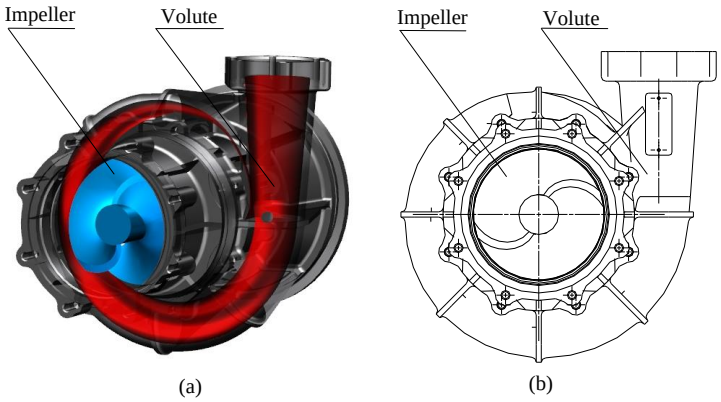

Figure 1. Final pump configuration: (**a**) overall layout; (**b**) overall top view.

Preprints (www.preprints.org) | NOT PEER-REVIEWED | Posted: 9 January 2020 doi:10.20944/preprints202001.0071.v1

Peer-reviewed version available at Energies 2020, 13, 919; doi:10.3390/en13040919

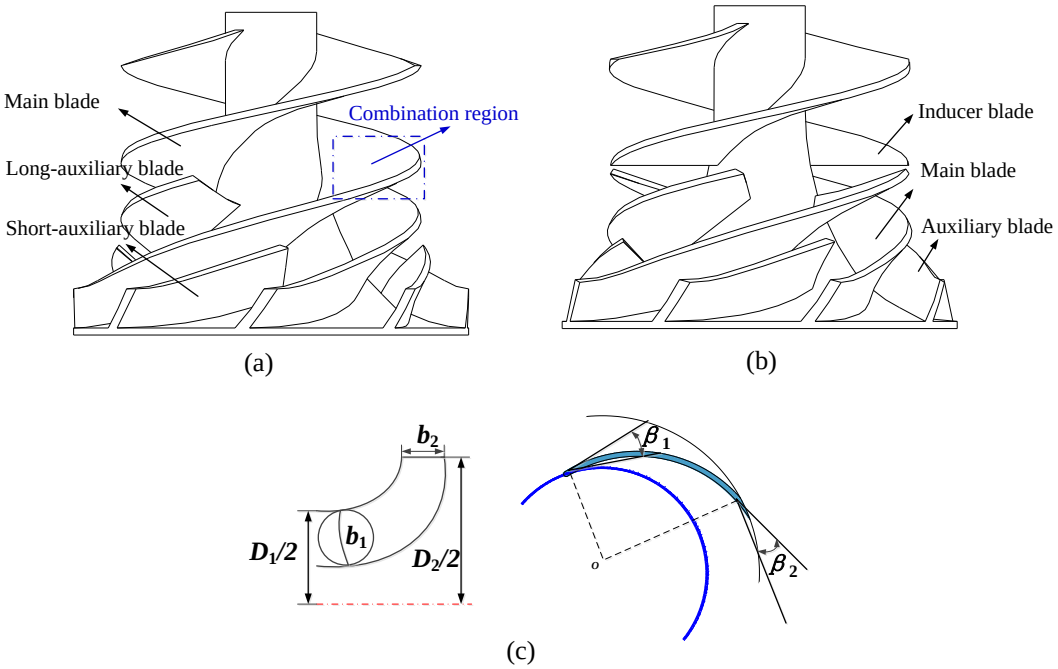

Figure 2. Shapes of combination and conventional impellers: (**a**) combination impeller; (**b**) conventional impeller; (**c**) main geometrical parameters.

In this paper, the volutes of two pumps are same. The cross-section of volute is a circular shape, and its diameter is alternative at different radian along the base circle. Figure 3 illustrates the geometric drawing process of volute.

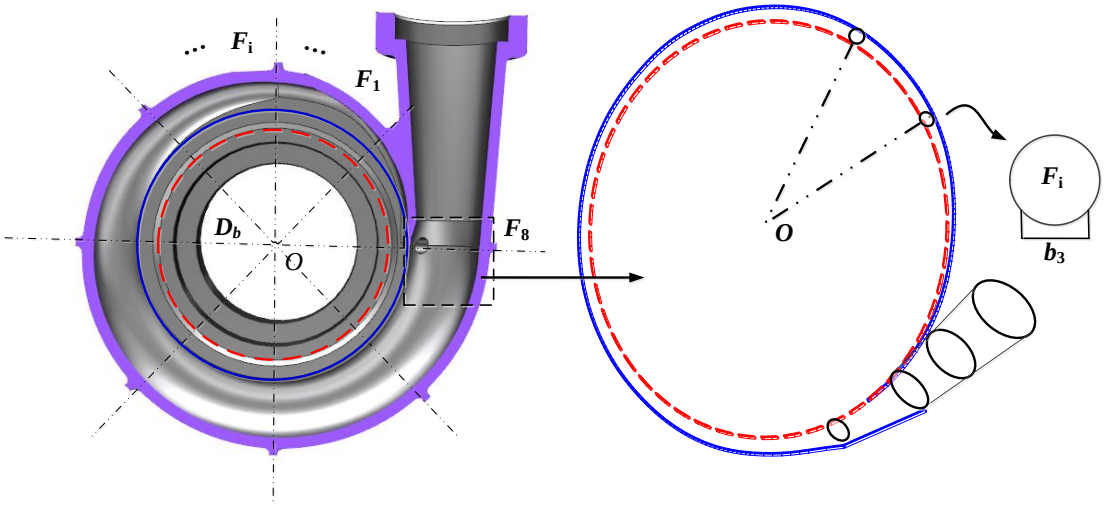

Figure 3. Geometric drawing process of volute.

The main geometrical parameters of the pump are determined according to Table. 1 and presented in Table 2. The inlet and outlet impeller diameters are denoted by D_1 and D_2, b_1 and b_2 represent inlet and outlet blade widths, leading and trailing edge angles are expressed by β_1 and β_2. And D_b is diameter of base circle, b_3 is inlet width of volute, F_8 represents eighth section area of volute.

Table 2. The main geometrical parameters of the pump

Parameters	Value
D_1(mm)	89
b_1(mm)	9.8
b_2(mm)	11
β_1(°)	22
β_2(°)	30
D_2(mm)	117
D_b(mm)	123
b_3(mm)	15
F_8(m²)	78

2.3. 3-D model

The 3-D models of two impellers are established with basic B-spline modeling method by commercial software, i.e., UG. Figure 4 shows the 3-D models of combination impeller, conventional impeller, and volute.

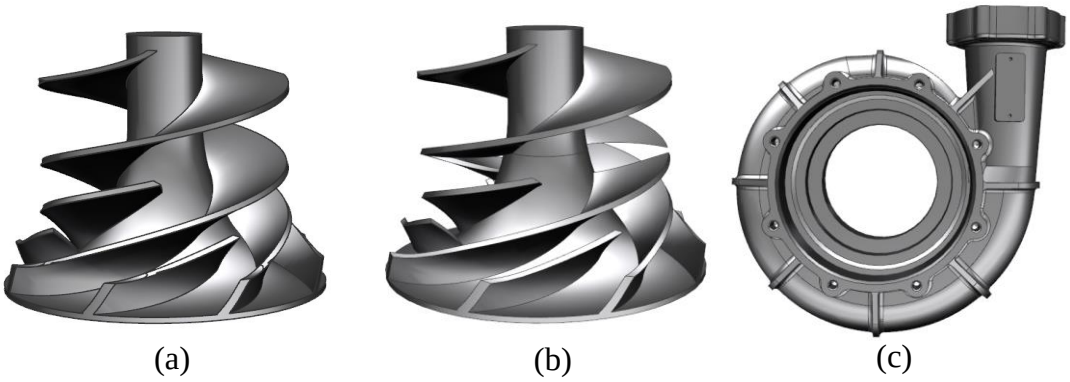

Figure 4. 3-D models: (**a**) combination impeller; (**b**) conventional impeller; (**c**) volute.

3. Validation study

In this section, in order to further validate the applicability of CFD methodology in this paper, a validation study is given to ensure the reliability of results. A series of numerical simulations for studied centrifugal pump are performed using different grid-schemes, in order to confirm the independence of determined mesh grid. Then, comparing the results between simulation and experiment, the effectiveness of selected turbulence model is conducted.

3.1. Mesh model and check of grid independence

The computational domain consists of two parts: impeller and volute. The mesh grids are generated by means of commercial software, i.e., PUMPLINX. In order to assure simulation stability and precision, unstructured mesh with good adaptability has been used to divide the computational domain. Figure 5 presents details of the generated mesh grids, and the mesh model of pump is illustrated in Fig. 5(a). Because of the complex flow passage structure in the volute tongue and impeller inlet, the two domains are discretized into refined mesh grids, as shown in Figs. 5(b) and 5(c).

Preprints (www.preprints.org) | NOT PEER-REVIEWED | Posted: 9 January 2020 doi:10.20944/preprints202001.0071.v1

Peer-reviewed version available at Energies 2020, 13, 919; doi:10.3390/en13040919

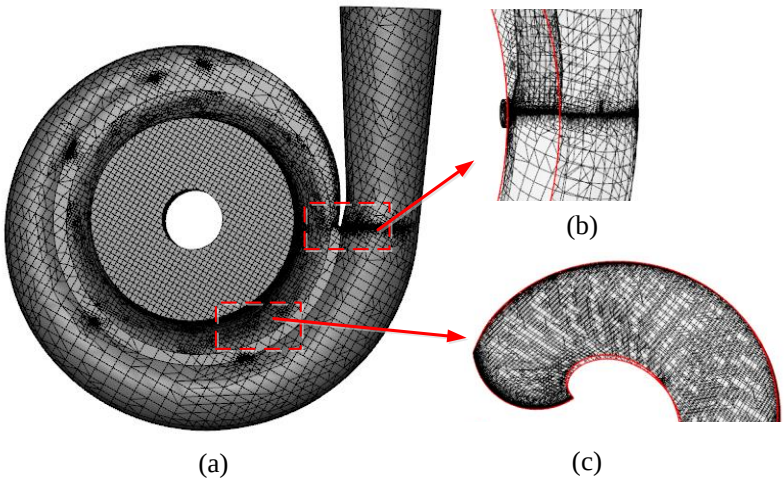

Figure 5. Details of the generated mesh grids: (**a**) mesh model of pump; (**b**) refined mesh model in volute tongue; (**c**) refined mesh model in impeller inlet.

Theoretically, the simulation errors will decrease gradually with increase of grid number; however, too many grids would pose prohibitive demands on computational resources and time [28]. So, different grid numbers are examined to ensure that the numerical solution is independent. Consequently, three grid-schemes named Grid-1, Grid-2 and Grid-3 are used for flow calculations. The grid numbers are 193268, 341456 and 721138 respectively. And the corresponding maximum cell sizes are 0.07mm, 0.05mm and 0.02mm. The pump head and efficiency at different flow rates of $0.8Q_d$, $1.0\ Q_d$, $1.2\ Q_d$ are predicted. The results are shown in Table 3.

Table 3. Pump performance of different mesh elements

Item	Pump	H			η_v		
		$0.8Q_d$	**1. Q_d**	**$1.2Q_d$**	**$0.8Q_d$**	**$1.0Q_d$**	**$1.2Q_d$**
Grid-1	193268	135	131	121	0.598	0.611	0.622
Grid-2	341456	140	133	124	0.643	0.65	0.646
Grid-3	721138	141	134	123	0.644	0.651	0.645

It indicates that the results are influenced gradually by increasing the grid numbers, and the overall difference is within 2%. The head and efficiency of Grid-1 are biggest among three grid-schemes, and the results of Grid-2 and Grid-3 are close together. Due to that the simulation results tend to be a relative constant value, the grid number has a slight effect on the pump head and efficiency. Therefore, Grid-2 is finally selected in the following simulations, because of its solution efficiency.

3.2. Numerical method and simulation conditions

Numerical simulation is performed by commercial software, i.e., PUMPLINX. The software provides a number of turbulence models. In this paper, the RNG κ-ε turbulence model [29] is selected to simulate flow field and predict external performance. The numerical simulation is based on the following conditions:

- The inlet boundary is set to be the pressure conditions, of which the total pressure is prescribed. A given mass flow is imposed at the outlet boundary.
- Fluid in the centrifugal pump is aero-fuel with a density of 779kg/m^3. The environment temperature for all the regions is set as 20°C and the kinematic viscosity is 1.48 m^2/s.
- The rotating domain of impeller is coupled to the stationary domain using the rotating reference frame method. The interface between impeller and volute is connected by the technique of frozen rotor method. Moreover, the solid walls such

Peer-reviewed version available at Energies 2020, 13, 919; doi:10.3390/en13040919

as blade, hub and shroud satisfy the non-slip condition, and they are assumed to be adiabatic.

- The pressure-velocity coupling equation is solved through the SIMPLE algorithm, and the convergence precisions of all residuals are below criterion of 1×10^{-5}.

3.3. Turbulence model verification

The incompressible continuity equation and Reynolds time averaged Navier–Stokes equation are solved by RNG k-ε turbulence model. The simulations are carried out at different flow rates, while the rotor speed is set as Nd. In order to verify the feasibility of selected model for pump simulation, an experimental pump is manufactured and tested in a pump company in Shaanxi Province, where the company is a participant in this paper (the information of experiment is shown in section 5). Based on simulation and experiment results, the head H and efficiency ηv of the centrifugal pump are predicted and obtained as:

$$H = \frac{p_c - p_{in}}{\rho g} + \Delta h \tag{1}$$

where P_{in} is the pump inlet pressure, P_c is the pump outlet pressure, and Δh is height difference between pump inlet and outlet.

$$\eta_v = \frac{\rho g Q H}{P \times 1000} \tag{2}$$

where P is the shaft power.

The predicted H and η_v of simulation are in acceptable agreement with experiment at different flow rates. The minimum relative errors between simulation and experiment are 0.8% and 1.2% for head and efficiency, so they nearly coincide at Q_d. The maximum relative errors are within 5% when the pump is operating at the low flow rates. Therefore, the performance of studied pump can be credibly predicted using CFD through the setting numerical method with RNG k-ε turbulent model.

4. Simulation results and discussions

In this section, in order to obtain the detailed flow characteristics and demonstrate the pump performances of studied pump, RNG κ-ε turbulence model is selected in the following simulations. Firstly, static pressure and relative velocity distributions of the studied pump at the axial section are demonstrated in Fig. 6. Secondly, the effects of combination impeller on the flow flied inside impeller and volute are illustrated in Figs. 7, 8, 9, and 10, respectively. Finally, under the simulation conditions, the external performances of pump with combination and conventional impeller are predicted and compared, shown in Fig. 11.

4.1. Flow characteristics in detail of the studied pump

Flow field in the pump is simulated at different flow rates. Figure 6 indicates static pressure and relative velocity distributions at the three flow rates ($Q = 0.8Q_d$, $1.0Q_d$, $1.2Q_d$), when the pump is operating at the nominal rotor speed N_d.

As shown from Fig. 6(a) to 6(c), the static pressure distributions show that the pressure increases gradually from pump inlet to outlet, and the minimum pressure occurs at the leading edge of blade suction surface. The pressure gradient distributes similarly between the two blade surfaces. However, caused by the action of fluid motion, the pressure is higher on pressure surface than that on suction surface at the same radius. Unfortunately, a small area of impeller outlet appears secondary flow loss. Meanwhile, asymmetry flow fields emerge in each impeller channels, and it performs more strictly at a larger flow rate. Besides, due to the rotor-stator interaction, an asymmetry flow is also observed in the volute. Furthermore, the pressure distribution in the channel nearby the volute tongue presents severely because of the flow obstruction, where a large pressure gradient appears at the large rate. Note that the change trend of pressure distribution is consistent at the five flow rates.

Preprints (www.preprints.org) | NOT PEER-REVIEWED | Posted: 9 January 2020 doi:10.20944/preprints202001.0071.v1

Peer-reviewed version available at Energies 2020, 13, 919; doi:10.3390/en13040919

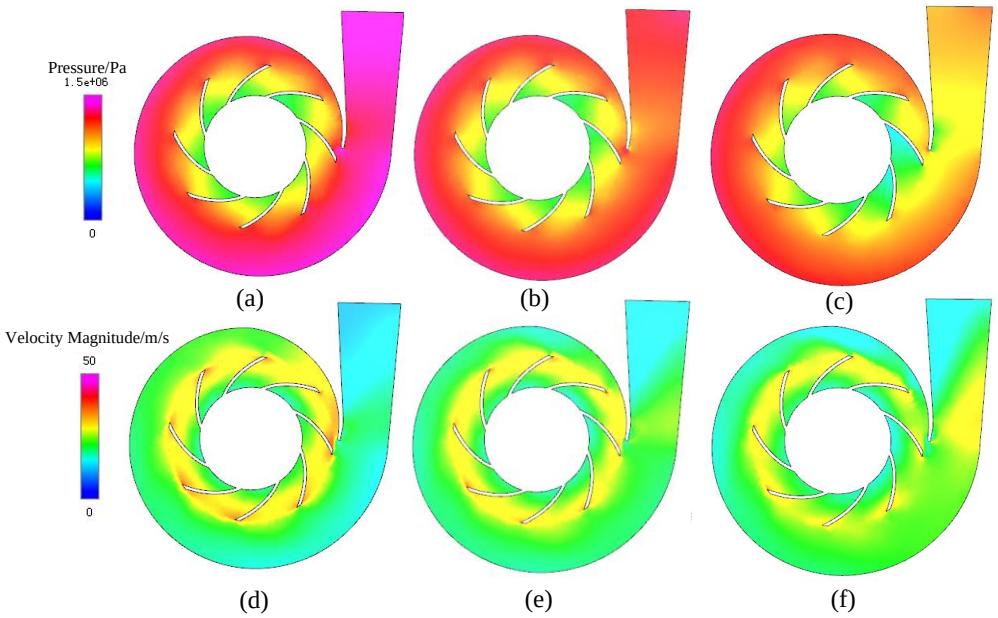

Figure 6. Static pressure and relative velocity distributions at the axial section: (**a**) static pressure, $0.8Q_d$; (**b**) static pressure, $1.0Q_d$; (**c**) static pressure, $1.2Q_d$; (**d**) relative velocity, $0.8Q_d$; (**e**) relative velocity, $1.0Q_d$; (**f**) relative velocity, $1.2Q_d$.

The relative velocity distributions of pump are demonstrated in Figs. 6(d), 6(e) and 6(f). It can be seen that the relative velocity in the pump distribute uniformly. The change trends of velocity distributions are consistent at the different flow rates, where the velocity increases in the impeller and decreases in the volute gradually. The minimum velocity with a gradient appears at impeller inlet. And the velocity on pressure surface is higher than that on suction surface. Same as pressure distribution, the velocity near the volute tongue presents severely. It will lead to a certain hydraulic loss.

Relying on the observations above, we can conclude that the pressure gradient appears on the blade surfaces. Asymmetry flow fields emerge in each impeller channels. The hydraulic loss exists within a certain region in the impeller inlet, impeller outlet and volute tongue, respectively. Therefore, some flow instabilities exist in the centrifugal pump, which is coincident with the conclusion indicted in [30, 31, 32].

4.2. Effects of combination impeller on the flow field inside impeller and volute

To confirm the effect of combination impeller on the flow field inside impeller and volute, simulation results of static pressure, relative velocity vector and fluid streamline are displayed in Figs. 7, 8, 9 and 10. Here, the pump is operating at three flow rates ($Q = 0.8Q_d$, $1.0Q_d$, $1.2Q_d$) and nominal rotor speed N_d.

In Fig. 7, it shows the comparisons of static pressure distributions at axial section between combination and conventional impellers. In impeller, the static pressure increases from impeller inlet to outlet at the three flow rates, and it distribute uniformly at the two blade surfaces. Moreover, the pressure gradient of combination impeller is higher than that of conventional impeller, which is observed more obviously at the lower flow rate. So, it may improve the utilization of the kinetic energy by combination impeller. Additionally, attributed to jet-wake flow at impeller outlet, a certain secondary flow loss both appears at the two impellers. The corresponding area of secondary flow is lower in combination impeller. On the other hand, it is obvious that the asymmetry flow gets better in the combination impeller passage, so a less local loss is realized. In volute, pressure decreases with increase of flow rate in all the cases, while it increases along the volute to pump outlet. So, the kinetic energy can be converted into static pressure as few loss as possible. Compared to conventional impeller, the pressure distribution of combination impeller is more uniform inside

Peer-reviewed version available at Energies 2020, 13, 919; doi:10.3390/en13040919

volute. Unfortunately, due to the jet-wake flow from impeller outlet, an asymmetry flow appears near the interface between impeller and volute. So, there is a certain pressure loss inside volute. It is also found that the maximum of pressure loss appears in the volute tongue. The extent of pressure loss reduces as the use of combination impeller, which means the effect of rotor-stator interaction gets weak. Clearly, the combination impeller can effectively regulate the flow inabilities in volute tongue.

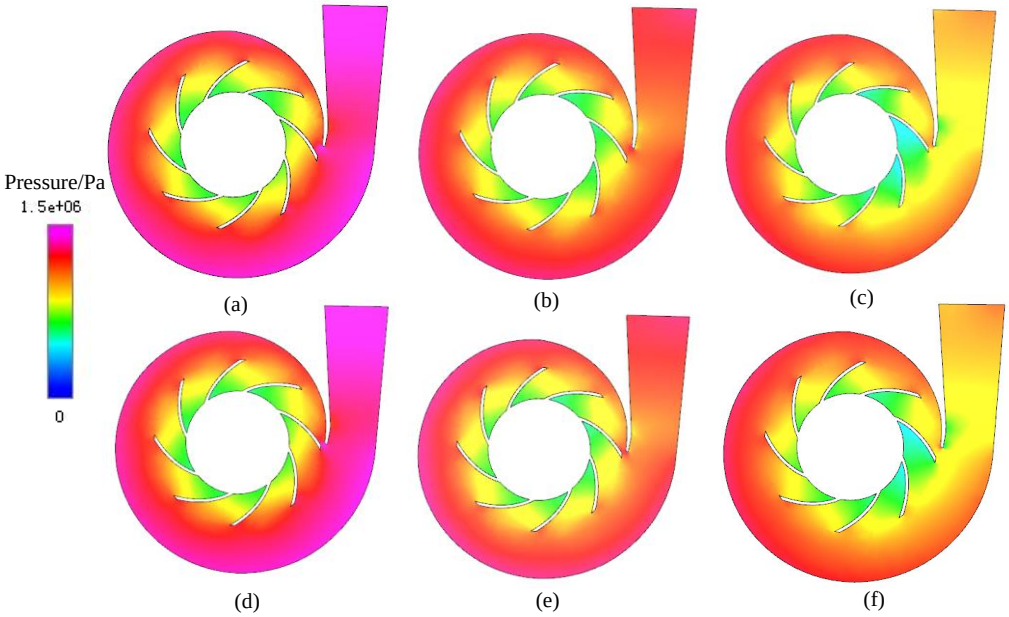

Figure 7. Static pressure and relative velocity distributions at the axial section: (**a**) combination impeller, 0.8Q_d; (**b**) combination impeller, 1.0Q_d; (**c**) combination impeller, 1.2Q_d; (**d**) conventional impeller, 0.8Q_d; (**e**) conventional impeller, 1.0Q_d; (**f**) conventional impeller, 1.2Q_d.

At the moment, we are unable to estimate flow characteristics at the combination region in impeller quantitatively. However, we can have a qualitative assessment by observing the location and size of separation zone alternatively. For such case, the static pressure distributions at radial section of combination and conventional impellers are shown in Fig. 8. So, the effect of combination impeller on the flow field in the combination region can be illustrated. The fuel is introduced into pump inlet, and then its pressure increases from impeller inlet to volute. The pressure is highest at the small flow rate with a largest gradient among the five flow rates. However, a vortex flow appears in the combination region which leads a certain vortex loss. Particularly, the impeller efficiency can be improved by decreasing the vortex loss in the region with the combination impeller. So, it indicates that it is effective for the centrifugal pump to control the flow characteristics by combination impeller.

To observe the velocity distribution clearly, the velocity vector at axial section is demonstrated in Fig. 9. The velocity increases from impeller inlet to outlet at the five flow rates, and it distribute uniformly at blade surfaces. However, at impeller outlet, a small area appears obvious high-velocity flow patterns. The region is smaller in combination impeller than that in conventional impeller, so it is found that combination impeller can decrease hydraulic loss at impeller outlet. Furthermore, it is inevitable for impeller to occur a back flow region because of the circumferential velocity in impeller. A back flow appears at the inlet of pressure suction which occupies a majority of impeller channel. Consequently, the fluid flows obstructively to impeller outlet due to the limited region near suction side. It has an adverse effect on the hydraulic performance. In two impellers, the back flow region near the long-blade pressure side is pushed to mid-part. Distinctively, it becomes smaller in combination impeller. At the large flow rate, it can be seen that the back flow region between long-blade pressure side and mid-blade suction side has already disappeared in combination

Preprints (www.preprints.org) | NOT PEER-REVIEWED | Posted: 9 January 2020 doi:10.20944/preprints202001.0071.v1

Peer-reviewed version available at Energies 2020, 13, 919; doi:10.3390/en13040919

impeller. In addition, when fuel flows into volute, the velocity decreases gradually because of the diffusion structure of volute. The velocity decreases along the volute to diffuser outlet at the five flow rates. Obviously, attributed to the jet-wake flow at the impeller outlet, an obvious high-velocity flow patterns appears in the region. Compared to conventional impeller, the area is smaller in combination impeller. Consequently, it illustrates that it is helpful to reduce the hydraulic loss in volute for the aero-fuel centrifugal pump by using the combination impeller.

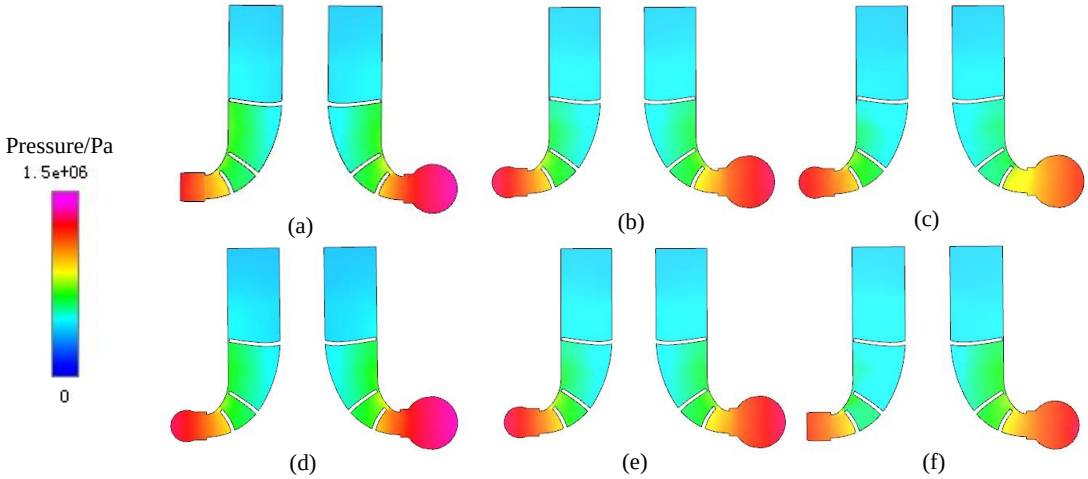

Figure 8. Comparisons of static pressure distributions at radial section between combination impeller and conventional impeller: (**a**) combination impeller, 0.8Q_d; (**b**) combination impeller, 1.0Q_d; (**c**) combination impeller, 1.2Q_d; (**d**) conventional impeller, 0.8Q_d; (**e**) conventional impeller, 1.0Q_d; (**f**) conventional impeller, 1.2Q_d.

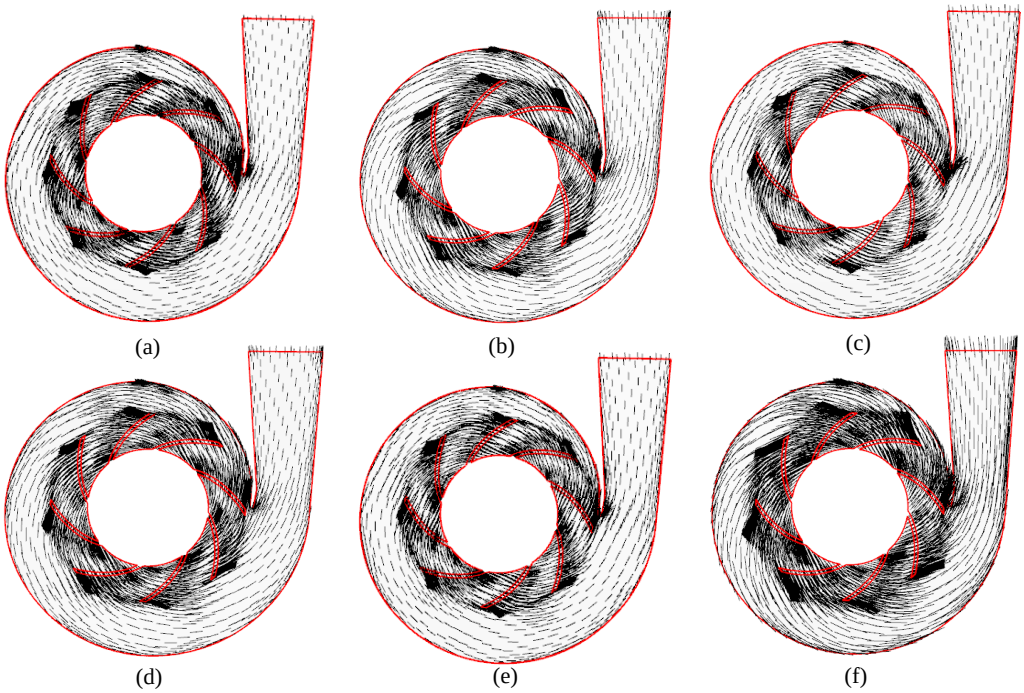

Figure 9. Comparisons of velocity vectors at axial section between combination impeller and conventional impeller: (**a**) combination impeller, 0.8Q_d; (**b**) combination impeller, 1.0Q_d; (**c**) combination impeller, 1.2Q_d; (**d**) conventional impeller, 0.8Q_d; (**e**) conventional impeller, 1.0Q_d; (**f**) conventional impeller, 1.2Q_d.

Preprints (www.preprints.org) | NOT PEER-REVIEWED | Posted: 9 January 2020 doi:10.20944/preprints202001.0071.v1

Peer-reviewed version available at Energies 2020, 13, 919; doi:10.3390/en13040919

To uncover the detailed flow characteristics in impeller and volute legibly, the fluid pathlines are illustrated in Fig. 10. The pathlines exhibit a helix pattern in the suction pipe in all the cases, and the rotational direction of fluid is clockwise. The helix angle is decreased with increase of flow rate, and it is smaller in the combination impeller than that in conventional impeller. So, the swirling flow in the suction pipe is nearly disappeared in combination impeller. It ensures that the inlet operating condition is acceptable. Moreover, at the combination region, it is obviously observed that the pathlines distributes more uniformly in combination impeller, so that the hydraulic energy can be utilized more effectively. Despite of the above superiority of pathlines in combination impeller, a certain flow loss occurs in impeller outlet, which is attributed to the secondary flow. In volute pipe, streamlines also exhibit a helix pattern in all the cases. Nevertheless, a swirling flow in volute is observed in volute tongue, and it performs seriously in conventional impeller.

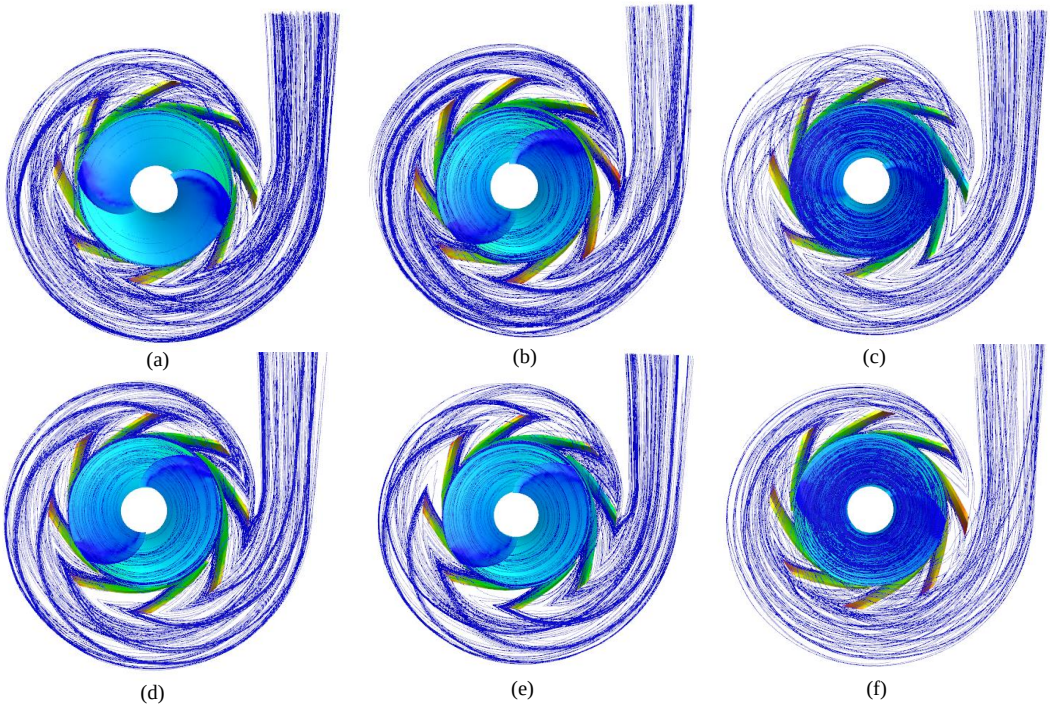

Figure 10. Comparisons of pathlines between combination impeller and conventional impeller: (**a**) combination impeller, 0.8Q_d; (**b**) combination impeller, 1.0Q_d; (**c**) combination impeller, 1.2Q_d; (**d**) conventional impeller, 0.8Q_d; (**e**) conventional impeller, 1.0Q_d; (**f**) conventional impeller, 1.2Q_d.

4.3. Effects of combination impeller on the external performance

According to the above analysis, it is concluded that the combination impeller has a crucial impact on the flow characteristics in certain regions, such as: impeller inlet, impeller outlet and volute tongue. In order to identify the flow characteristics quantitatively, the external performances of the two pumps are predicted according to Eq. (1) and Eq. (2). Figure 11 illustrates the comparisons of performance curves (Q-H, Q-η_v). The change trends of head H and efficiency η_v are relatively consistent to each other. Importantly, the best efficiency point (BEP) occurs at Q_d (77000m3 · h-1), where the highest efficiency and head of the pump with combination impeller are 0.65 and 133m. So, the external performances of studied pump are in good agreement with performance requirements. And they are both higher than those of the pump with conventional impeller. In addition, the high efficiency region of the pump with combination impeller is wider near Q_d. So, it is able to operate stably over the entire operating range, especially at the off-nominal flow rates.

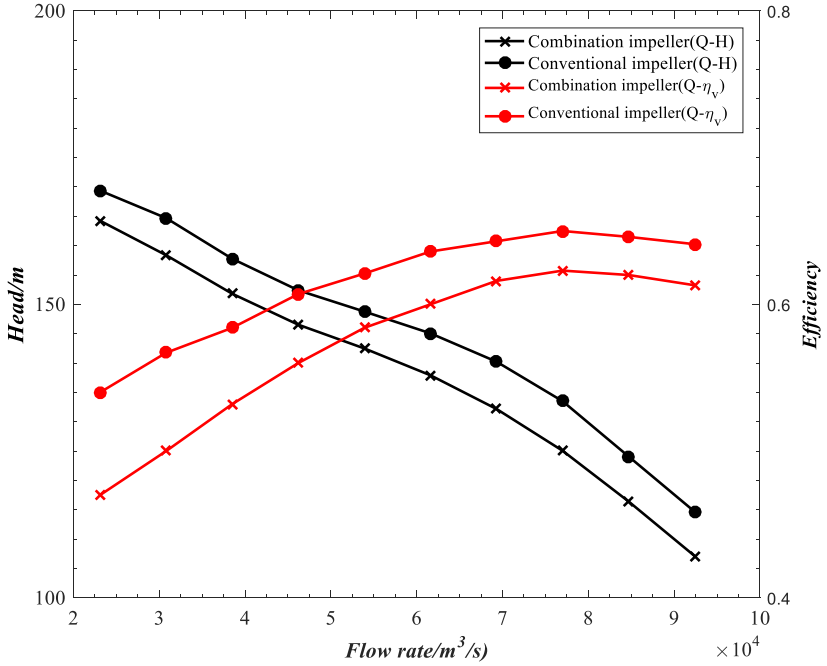

Figure 11. Comparisons of the performance curves.

Consequently, it is a promising approach in improving the external performance by applying the combination impeller to an aero-fuel centrifugal pump, which is corresponding to the effect on the flow field.

5. Experimental studies for external performance

In this section, in order to verify the feasibility of simulation and realize the external performance of studied pump, the external performance experiments are carried out on the experimental setup in the following experimental studies. Firstly, the experimental pump, schematic diagram and experimental apparatus are demonstrated in Fig. 12. Then, the experiment results of studied pump are illustrated at different flow rates, as shown in Fig. 13.

5.1. Experimental setup

Figure 12 shows the experimental setup. The experimental pump is manufactured in a pump company in Shaanxi Province, as shown in Fig. 12(a). The schematic diagram is shown in Fig. 12(b). Fig. 12(c) illustrates the experimental apparatus. It consists of (1) fuel supply section: fuel tank, crude fuel filter and inlet regulating valve; (2) pump section: experimental centrifugal pump and electric motor; (3) fuel regulating section: pressure sensor, pressure gauge, flow meter, temperature sensor, electric throttle valve, manual throttle valve and overflow valve.

The flow rates and rotor speeds of the pump are obtained under the standard atmosphere condition, and static pressures on the pump inlet and outlet are measured by related pressure sensors to predict the pump head.

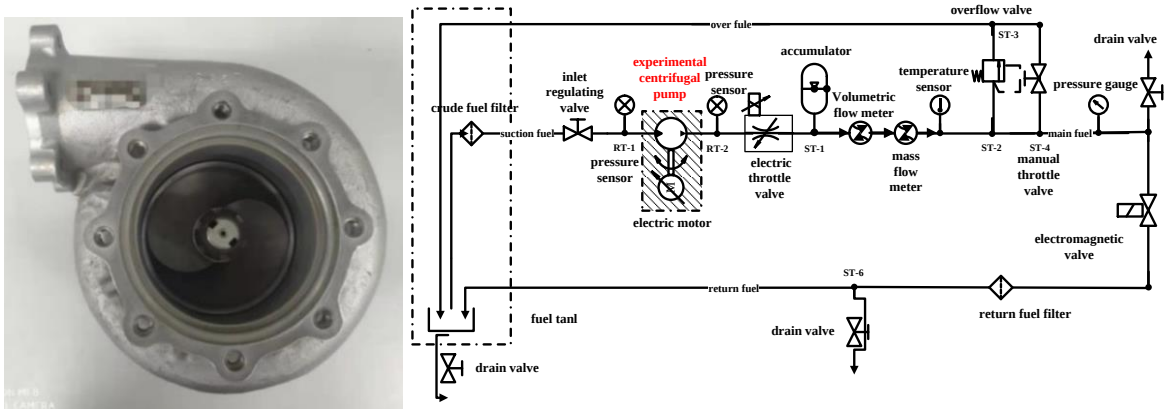

(a) (b)

(c)

Figure 12. Experimental setup: (**a**) experimental pump; (**b**) schematic diagram.

5.2. External performance test

Figure 13 shows the external performance curves for the studied pump under different operating conditions.

The head decreases with increase of flow rate and rotor speed. When the pump is operating at N_d, the results between simulation and experiment are very close within a relative error of 5%. It illustrates that the external performance of experiment is in good agreement with that of simulation. Importantly, the BEP occurs at Q_d (77000L/h) and the highest efficiency of the pump is 0.65, which is nearly coincident with the conclusion indicted in section 4.4. In addition, the high efficiency region is wide near the nominal operating point. Therefore, the studied centrifugal pump is stable over the entire operating range, especially under the off-nominal operating conditions.

It is verified that the aero-fuel centrifugal pump with combination impeller has an ability to achieve the technical requirements at a large nominal operating flow rate (77000L/h), and it has an active effect on the energy-saving due to its high efficiency working.

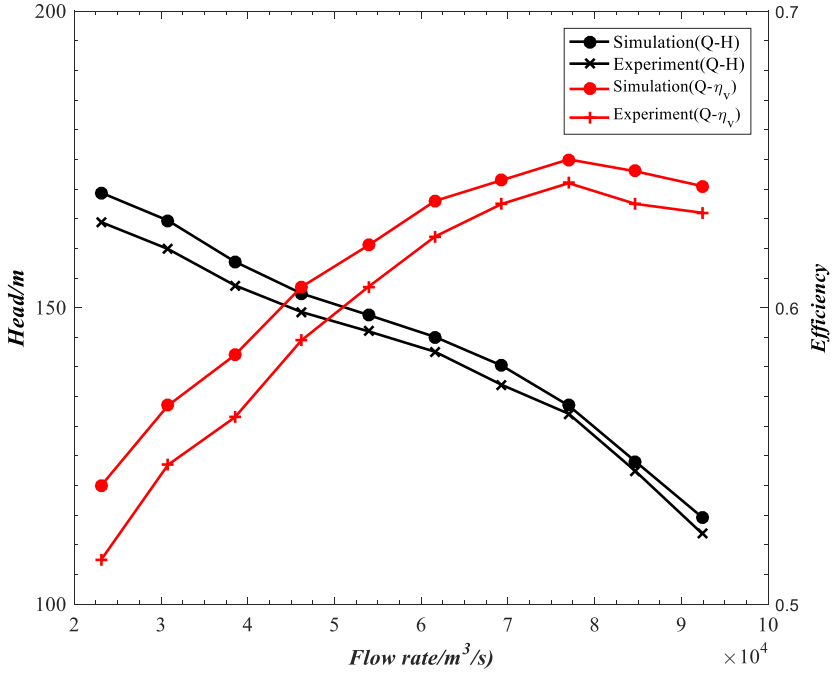

Figure 13. External performance curves for the studied pump.

5. Conclusions

In this paper, the flow field and external performance of an aero-fuel centrifugal pump with a combination impeller are conducted by numerical simulation and experiment. The numerical method is validated by comparing simulation results with own experimental data, then the flow field is simulated and external performance is predicted. The following conclusions can be drawn:

(1) The results of simulation and experiment are very close within a relative error of 5% when the pump is operating at N_d. It illustrates that the external performances of simulation are in good agreement with experiment.

(2) The hydraulic losses inside impeller and volute can be decreased when the pump is equipped with the combination impeller. Especially, the flow instabilities in impeller inlet, impeller outlet and volute tongue are significantly regulated. In addition, the predicted head and efficiency of the pump with combination impeller are both higher than those of the pump with conventional impeller. It illustrates that it is a promising approach in ameliorating flow field and improving external performance by applying a combination impeller to an aero-fuel centrifugal pump.

(3) The BEP of the pump with combination impeller occurs at Q_d (77000L/h) and the highest efficiency is 0.65. It is stable with high efficiency over the entire operating range. It illustrates that the pump has an ability to achieve the technical requirements at the large nominal operating flow rate (77000 L/h), and it has an active effect on the energy-saving because of its high efficiency working.

The demonstrated results show the effectiveness and reliability of the studied pump to regulate the flow field and external performance. However, anti-cavitation of the pump has not yet been considered, so it is one of our future works.

Author Contributions: Data curation, Xin Wang; Formal analysis, Yue Wang; Funding acquisition, Wancheng Wang; Investigation, Jia Li; Methodology, Baibing Chen; Resources, Xiaolong Chen; Writing – original draft, Jia Li; Writing – review & editing, Jia Li.

Funding: This research was funded by the National Natural Science Foundation of China (No. 51506177) and the Fundamental Research Funds for the Central Universities of Chang' an University(No. 300102259101).

Acknowledgments: The authors gratefully acknowledge the financial support of the National Natural Science Foundation of China, the Fundamental Research Funds for the Central Universities of Chang' an University.

Conflicts of Interest: The authors declare no conflict of interest.

References

1. Liu S. Q. Investigation of centrifugal pump used as aero-engine main fuel pump. *Aeroengine*. **2006**, 32, 43-45.
2. Sutton G. P. History of Liquid Propellant Rocket Engines. Virginia: American Institute of Aeronautics and Astronautics. **2006**.
3. Koyama N. Utilization of Centrifugal Pumps Used as Hydraulic Turbines. *Journal of the Japan Society of Mechanical Engineers*. **1971**, 74: 1584-1587.
4. Arriaga M. Pump as turbine–a pico-hydro alternative in Lao People's Democratic Republic. *Renewable Energy*. **2010**, 35: 1109–1115.
5. Petrone G.; de Nicola C.; Quagliarella D.; Witteveen J. Wind turbine performance analysis under uncertainty. *In Proc. 49th AIAA Aerospace Sciences Meeting including the New Horizons Forum and Aerospace Exposition*. **2011**: 544-556.
6. Zhang J. F. Numerical and experimental investigation on configuration optimization of the large-size ionic wind pump. *Energy*. **2019**, 171: 624-630.
7. Stepanoff A. J. Centrifugal and Axial Flow Pumps, Design and Applications. New York: John Wiley and Sons. **1957**.
8. Shen Z. S.; Chu W.; Li X.; Dong W. Sediment erosion in the impeller of a double-suction centrifugal pump – A case study of the Jingtai Yellow River Irrigation Project, China. *Wear*. 2019, 422: 269-279.
9. Fan S. Q. Aeroengine Control. Xi'an: Northwestern Polytechnical University Press, 2008.
10. Jiang Q. F.; Heng Y. G.; Liu X. B.; Zhang W. B. A review of design considerations of centrifugal pump capability for handling inlet gas-liquid two-phase flows. *Energies*. **2019**, 12: 1078.
11. Han W., Nan L. B., Su M.; Yu C. Research on the prediction method of centrifugal pump performance based on a double hidden layer BP neural network. *Energies*. **2019**, 12: 2709.
12. Yan P.; Chu N.; Wu D.; Cao L. Computational fluid dynamics-based pump redesign to improve efficiency and decrease unsteady radial forces. *Journal of Fluids Engineering*. **2017**, 139: 011101.
13. Cao L.; Zhang Y.; Wang Z.; Xiao Y. Effect of axial clearance on the efficiency of a shrouded centrifugal pump. *Journal of Fluids Engineering*. **2015**, 137: 071101.
14. Dönmez A. H., Yumurtacı Z.; Kavurmacıoğlu L. The effect of inlet blade angle variation on cavitation performance of a centrifugal pump: a parametric study. *Journal of Fluids Engineering*. **2019**, 141: 021101.
15. Zhou L.; Shi W.; Li W.; Agarwal R. Numerical and experimental study of axial force and hydraulic performance in a deep-well centrifugal pump with different impeller rear shroud radius. *Journal of Fluids Engineering*. **2013**, 135: 104501.
16. Jafarzadeh B.; Hajari A.; Alishahi M. M.; Akbari M.H. The flow simulation of a low-specific-speed high-speed centrifugal pump. *Applied Mathematical Modelling*. **2011**, 35: 242–249.
17. Shojaeefard M. H.; Tahani M.; Ehghaghi M. B.; Fallahian M. A. Numerical study of the effects of some geometric characteristics of a centrifugal pump impeller that pumps a viscus fluid. *Computers & Fluids*. **2012**, 60: 61–70.
18. Guo X. M.; Zhu L.; Zhu Z. C.; Cui B. Numerical and experimental investigations on the cavitation characteristics of a high-speed centrifugal pump with a splitter-blade inducer. *Journal of mechanical science and technology*. **2015**, 29: 259–267.
19. Luo X.; Zhang Y.; Peng J.; Xu H. Impeller inlet geometry effect on performance improvement for centrifugal pumps. *Journal of mechanical science and technology*. **2018**, 22: 1971–1976.
20. Lundgreen R. K.; Oliphant K.; Maynes D.; Gorrell S. E. High suction performance pumps with large inlet blade angles and an integrated stability control device. *In Proc. 52nd AIAA/SAE/ASEE Joint Propulsion Conference*. **2016**: 4985-4999.
21. Chen H. X.; He J. W.; Liu C. Design and experiment of the centrifugal pump impellers with twisted inlet vice blades. *Journal of Hydrodynamics*. **2017**, 29: 1085-1088.
22. Ayad A. F.; Abdalla H. M.; Aly A. A. E. A. Effect of semi-open impeller side clearance on the centrifugal pump performance using CFD. *Aerospace Science and Technology*. **2015**, 47: 247-255.
23. Yousef H.; Noorollahi Y.; Tahani M.; Fahimi R.; Saremian S. Numerical simulation for obtaining optimal impeller's blade parameters of a centrifugal pump for high-viscosity fluid pumping. *Sustainable Energy Technologies and Assessments*. **2019**, 34: 16–26.

24. Hong S. S.; Kim D. J.; Kim J. S.; Choi C. H. Study on inducer and impeller of a centrifugal pump for a rocket engine turbopump. *Proceedings of the Institution of Mechanical Engineers, Part C: Journal of Mechanical Engineering Science*. **2013**, 227: 311-319.
25. Guo X. M.; Zhu Z. C.; Shi G. P.; Yong H. Effects of rotational speeds on the performance of a centrifugal pump with a variable-pitch inducer. *Journal of hydrodynamics*. **2017**, 29: 854-862.
26. Li W. G. Effects of viscosity on turbine mode performance and flow of a low specific speed centrifugal pump. *Applied Mathematical Modeling*. **2016**, 40: 905-926.
27. Stechmann D. Design and analysis of a high-pressure turbopump at Purdue University. *In Proc. 51st AIAA/SAE/ASEE Joint Propulsion Conference*. **2015**: 4216-4240.
28. Wang C.; Shi W.; Wang X.; Jiang X. Optimal design of multistage centrifugal pump based on the combined energy loss model and computational fluid dynamics. *Applied Energy*. **2017**, 187: 10-26.
29. Song Y.; Fan H. G.; Zhang W.; Xie Z. F. Flow characteristics in volute of a double-suction centrifugal pump with different impeller arrangements. *Energies*. **2019**, 12: 669.
30. Tan L.; Zhu B. S.; Cao S. L.; Bing H. Influence of blade wrap angle on centrifugal pump performance by numerical and experimental study. *Chinese journal of mechanical engineering*. **2015**, 27: 171-177.
31. Ding H. C.; Li Z. K. The influence of blade outlet angle on the performance of centrifugal pump with high specific speed. *Vacuum*. **2019**, 159: 239-246.
32. Han X. D.; Kang Y.; Li D.; Zhao W. G. Impeller optimized design of the centrifugal pump: a numerical and experimental investigation. *Energies*. **2018**, 11: 1444.